1-1-2014

MRI distortion: considerations for MRI based radiotherapy treatment planning

Amy Walker
University of Wollongong, aw554@uowmail.edu.au

Gary P. Liney
University of Wollongong

Peter E. Metcalfe
University of Wollongong, metcalfe@uow.edu.au

Lois Holloway
University of Wollongong, loish@uow.edu.au

MRI distortion: considerations for MRI based radiotherapy treatment planning

Abstract

Distortion in magnetic resonance images needs to be taken into account for the purposes of radiotherapy treatment planning (RTP). A commercial MRI grid phantom was scanned on 4 different MRI scanners with multiple sequences to assess variations in the geometric distortion. The distortions present across the field of view were then determined. The effect of varying bandwidth on image distortion and signal to noise was also investigated. Distortion maps were created and these were compared to the location of patient anatomy within the scanner bore to estimate the magnitude and distribution of distortions located within specific clinical regions. Distortion magnitude and patterns varied between MRI sequence protocols and scanners. The magnitude of the distortions increased with increasing distance from the isocentre of the scanner within a 2D imaging plane. Average distortion across the phantom generally remained below 2.0 mm, although towards the edge of the phantom for a turbo spin echo sequence, the distortion increased to a maximum value of 4.1 mm. Application of correction algorithms supplied by each vendor reduced but did not completely remove distortions. Increasing the bandwidth of the acquisition sequence decreased the amount of distortion at the expense of a reduction in signal-to-noise ratio (SNR) of 13.5 across measured bandwidths. Imaging protocol parameters including bandwidth, slice thickness and phase encoding direction, should be noted for distortion investigations in RTP since each can influence the distortion. The magnitude of distortion varies across different clinical sites.

Keywords

treatment, planning, radiotherapy, mri, considerations, distortion

Disciplines

Engineering | Science and Technology Studies

Publication Details

Walker, A., Liney, G. P., Metcalfe, P. E. & Holloway, L. C. (2014). MRI distortion: considerations for MRI based radiotherapy treatment planning. Australasian Physical & Engineering Sciences in Medicine, 37 (1), 103-113.

MRI distortion: considerations for MRI based radiotherapy treatment planning

Authors:

Amy Walker[1,2]*, Gary Liney[1,2,3], Peter Metcalfe[1,2], Lois Holloway[1,2,3,4]

Affiliations:

1. Centre for Medical Radiation Physics, University of Wollongong, Wollongong, NSW 2522, Australia
2. Liverpool and Macarthur Cancer Therapy Centres and Ingham Institute, Liverpool, NSW 2170, Australia
3. South West Clinical School, University of New South Wales, Sydney, NSW 2052, Australia
4. Institute of Medical Physics, School of Physics, University of Sydney, Sydney, NSW 2006, Australia

*Corresponding Author:
Email: aw554@uowmail.edu.au
Phone: 0403521673
Key Words: MRI, geometric distortion, bandwidth, phantom, radiotherapy treatment planning

Abstract:

Distortion in magnetic resonance images needs to be taken into account for the purposes of radiotherapy treatment planning (RTP). A commercial MRI grid phantom was scanned on 4 different MRI scanners with multiple sequences to assess variations in the geometric distortion. The distortions present across the field of view were then determined. The effect of varying bandwidth on image distortion and signal to noise was also investigated. Distortion maps were created and these were compared to the location of patient anatomy within the scanner bore to estimate the magnitude and distribution of distortions located within specific clinical regions. Distortion magnitude and patterns varied between MRI sequence protocols and scanners. The magnitude of the distortions increased with increasing distance from the isocentre of the scanner within a 2D imaging plane. Average distortion across the phantom generally remained below 2.0 mm, although towards the edge of the phantom for a turbo spin echo sequence, the distortion increased to a maximum value of 4.1 mm. Application of correction algorithms supplied by each vendor reduced but did not completely remove distortions. Increasing the bandwidth of the acquisition sequence decreased the amount of distortion at the expense of a reduction in signal-to-noise ratio (SNR) of 13.5 across measured bandwidths. Imaging protocol parameters including bandwidth, slice thickness and phase encoding direction, should be noted for distortion investigations in RTP since each can influence the distortion. The magnitude of distortion varies across different clinical sites.

I. INTRODUCTION

There is a growing interest in utilising MRI for radiotherapy treatment planning (RTP). One of the main reasons for this is the superior soft tissue information that MRI can provide, improving the differentiation between various soft tissue structures and increased accuracy in volume delineation [1,2]. One of the potential issues in the radiotherapy community impacting on the more widespread uptake of MRI for RTP is geometric distortion within the image [3]. Changing the geometric integrity of the patient anatomy has the potential to affect the precision of beam targeting and dose calculations within radiotherapy treatment planning systems. This has the potential to result in variations in clinical outcomes. These distortions are caused by both system specific and patient related factors.

System specific distortions result from variations in the homogeneity of the main magnetic field (B_o) and the nonlinearities of the gradient coils within the scanner. The effects resulting from these intrinsic scanner components alone are reproducible for the same scan protocols, whilst varying between scanners due to variations in system specifications and performance [4].

The gradient coils allow for the localisation of a signal from within the body, enabling the anatomy to be visualised. Images are constructed on the premise that these gradients are linear and there is a homogeneous main magnetic field (B_0). In modern scanners there is a trade-off in gradient linearity to allow for utilisation of fast imaging sequences and stronger gradient strengths. Whilst such advances can reduce the effects of patient movement and increase patient comfort, the geometric distortions may be greater due to these gradient nonlinearities. This causes a mismapping of pixels, affecting the geometrical integrity of the resulting image. General specifications for scanner body gradient coils are that the gradient error should be less than 2% the gradient strength over a 40 cm diameter of spherical volume (DSV)[5]. Performance specifications of additional gradient coil inserts are characteristically less than this, which can lead to increased nonlinearity effects [5]. Altering parameters in the image protocol alters the dependence of the acquisition on the gradient coils and the main magnetic field, altering the distortion present in the image, based on the imperfections in these features.

There have been a number of different methods proposed for dealing with nonlinear gradient distortions for use in RTP. Many of these methods are based on obtaining phantom images with a known geometry and comparing the apparent position of structures within the MR image to the known point locations to create a distortion map across the field of view (FOV) [6-10]. After this, post-processing can be conducted in order to correct for the distortion based on these maps with the aim to reduce distortions below 2 mm. Distortions above 2 mm may need to be corrected for to ensure accurate radiotherapy treatment [11,8]. Any residual distortions would need to be considered when determining planning volumes to ensure that the target volume is covered [12]. This would depend on the location of the anatomical site and the magnitude of the distortions observed within that region of the scanner.

A more theoretical approach can be utilised by applying spherical harmonic deconvolution methods to correct for distortions within a specific device's FOV [13]. This method is the basis for the correction algorithms utilised on some commercial scanners and also includes a density correction for intensity variations caused by these distortions [11].

The homogeneity of the scanners B_0 field is another system property which can alter the distortion present in images. Main field homogeneity is measured in parts per million (ppm) over a DSV extending out from the scanner isocentre. Homogeneity values for current scanners are nominally 1.1 ppm across a 50 cm

DSV. For a 1.5 T scanner, this corresponds to a frequency offset of 70.2 Hz. Such homogeneity variations can create discrepancies in signal location and manifest as image intensity variations and distortions within the image.

While distortions are unwanted in any image, their impact is dependent on how the images are utilised. This paper evaluates geometrical inaccuracy with respect to the application of images for RTP purposes. Previous studies of MRI distortion investigating the use of MRI for radiotherapy for a number of anatomical sites have focused on one specific acquisition sequence [14,4,15,6,16,8,7,9,17]. These studies were also focused on anatomical locations which would be placed close to the centre of the scanner such as the prostate [2,16,8], head and neck [11,18,19] as well as stereotactic radiosurgery applications [20].

In this study, images of a test phantom were obtained in one imaging plane using a number of different clinical MRI protocols with varying selection parameters. Four MRI scanners from different centres were investigated. Differences in the magnitude and direction of the distortion between scanners and imaging protocols were assessed. This data was then compared to the location of anatomical sites which may be of interest when considering the use of MRI in RTP. This study also investigated the effects of varying bandwidth on distortion and SNR. By acquiring images at two different bandwidths it was also possible to estimate the homogeneity using the method described by Chen et al. [21]. This study only considered distortions from systematic factors. Patient related distortions were not addressed in this study.

II. MATERIALS AND METHODS

II.A. Phantom

To determine the distortion magnitude and pattern, MRIs of a FLUKE Biomedical phantom were acquired (Fig. 1). This commercially developed phantom conforms to the specifications as outlined in the AAPM nuclear magnetic resonance task group number 1 [22]. It is designed to enable the testing of uniformity and linearity of MRI scanners. The acrylic phantom has outer dimensions of 330 mm x 330 mm x 102 mm, with the grid region of dimensions 277 mm x 277 mm x 25 mm. Contained within this were 397 cylindrical grid points in a 20 x 20 2D grid layout, with three points removed for consistent orientation and alignment. The spacing between the axial centres of each grid point is approximately 15 mm, with each grid point having a diameter of 12 mm. The grid points were created by systematically placed holes milled into the acrylic structure. The holes were filled with saline to create the proton based signal detected by the MRI scanner. The centre of the phantom was aligned in the horizontal direction to the centre of the scanner. The vertical position of the phantom was determined by the fixed couch height of each scanner.

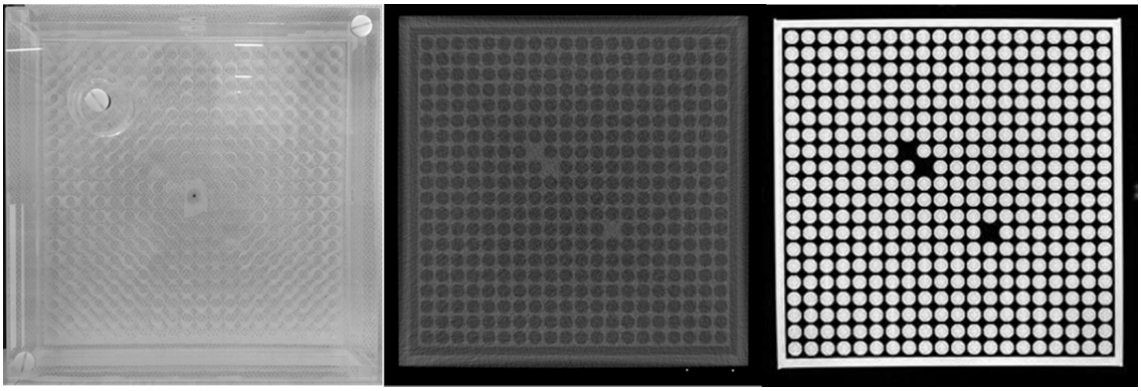

Fig. 1 From left to right: the phantom used for this study, CT scan of the phantom and a turbo spin echo image of the phantom

II.B. CT imaging procedure

A CT scan of the phantom was undertaken on a Siemens SOMATOM Sensation scanner. This was taken to be the 'gold standard' scan, assumed to have negligible distortion for determining the grid point locations. Scan parameters included a FOV of 500 mm, 512 x 512 matrix (spatial resolution 0.98 mm) and a slice thickness of 2 mm.

II.C. MR imaging procedure

Sequence comparisons

Measurements were made on four clinical MRI scanners, a 60 cm bore Intera Achieva Nova Dual 1.5 T (Philips Medical Systems, The Netherlands), a 60 cm bore MAGNETOM® Symphony Syngo 1.5 T, a 70 cm bore MAGNETOM® Verio 3 T and a 70 cm bore MAGNETOM® Skyra 3 T (Siemens Medical Systems, Erlangen, Germany). A number of sequences were investigated based on their clinical applications for radiotherapy treatment planning. Table 1 shows the acquisition details for each of these sequences. The sequences were matched as closely as possible on the different MRI scanners for comparative purposes.

To ensure set-up reproducibility on different scanners, round MRI non-magnetic multi-modality markers were fixed to the sides of the phantom and the laser system on the scanners used to align these markers to the scanner isocentre. Analysis of both CT and MR images were conducted on the axial image slice corresponding to the centre of the scanner and the central region of the phantoms grid structure. To overcome the issue of the rounded/padded couch, one of two approaches was taken, depending on the scanner.

For the Siemens 3 T Verio and the Philips 1.5 T scanners, the phantom was placed on a flat Styrofoam board to ensure its stability on the couch. The spine coil was removed on the Siemens 1.5 T Symphony and 3 T Skyra scanners, allowing for stable placement of the phantom as well as creating better alignment between the phantom centre and the scanner isocentre. The position of the phantom with respect to the scanner isocentre was noted so that all distortion measurements could be made with reference to the distance from this point. The vertical position of the phantom was dependent on the couch height.

For both the Siemens 3 T scanners, there was an option in the acquisition setup allowing for application of inbuilt gradient correction algorithms. The 2D algorithms were applied on these scanners, since the phantom design meant that distortion could only effectively be measured within a 2D imaging plane. For comparative purposes on the Siemens Verio 3 T scanner, phantom images were also analysed without the application of the 2D gradient correction algorithm. The images were initially acquired with the algorithm turned on. Once all of the sequences had been acquired and saved, non-corrected images were then obtained through post processing methods, by deselecting the 2D algorithm option in the control panel and resaving the image sets. The corresponding changes in distortion between the two modes of acquisition could then be determined.

Table 1 Parameters of the MRI acquisition sequences for which distortion was assessed

Scanner	Sequence	Weight type	2D/3D	TR/TE (ms)	FOV (mm)	Flip angle (^{o})	Slice thickness (mm)	Read out gradient direction	Pixel BW (Hz/pix)
Philips	Spoiled GRE	T1	3D	25/4.6	450 x 450	30	3	Row	131
(1.5T Intera Achieva)[a]	Spoiled GRE (In/Out of phase)	T1	2D	162.6/4.6	450 x 450	80	3	Column	1818
	Volume interpolated GRE (In/Out of phase)	T1	3D	7.0/4.8	450 x 450	9	4	Column	434
	Volume interpolated GRE	T1	3D	4.3/2.1	450 x 450	9	4	Column	434
	Single shot TSE	T2	2D	1500/120	450 x 450	124	4	Row	355
	3D TSE (Variable flip angle)	T2	3D	2000/350.8	450 x 450	120	5	Column	417
	TSE	T2	2D	4012.9/100	450 x 450	90	4	Row	191
Siemens	Spoiled GRE	T1	3D	7.2/2.8	450 x 450	20	1.3	Row	175
(1.5T Symphony Syngo)[b]	Spoiled GRE (In/Out of phase)	T1	2D	139/2.32	450 x 450	70	4	Column	390
	Single shot TSE	T2	2D	1890/115	450 x 450	120	4	Row	115

	3D TSE	T2	3D	1820/471	420 x 420	120	2.5	Row	125
	TSE	T2	2D	4550/127	450 x 450	120	4	Column	85
	TSE	T2	2D	4550/127	450 x 450	120	4	Row	85
	3D SE	T2	3D	9.4/4.8	420 x 420	20	5	Column	150
Siemens	Spoiled GRE	T1	3D	6.0/2.5	450 x 450	20	1.3	Row	399
(3T Verio)[c]	Spoiled GRE	T1	2D	167/2.5	420 x 420	70	4	Row	279
	Volume interpolated GRE (In/Out of phase)	T1	3D	4.4/2.5	450 x 365	9	3	Column	679
	Volume interpolated GRE	T1	3D	4.6/2.0	450 x 450	9	2	Row	401
	Single shot TSE	T2	2D	1890/119	450 x 450	120	4	Row	507
	3D TSE (Variable flip angle)	T2	3D	1280/90	450 x 450	120	2.5	Row	244
	TSE	T2	2D	5030/81	450 x 450	80	4	Row	228
Siemens (3 T Skyra)[d]	Spoiled GRE	T1	3D	5.7/2.5	340 x 340	20	3	Row	390
	Spoiled GRE	T1	2D	90/2.5	340 x 340	70	4	Row	280
	Volume interpolated GRE (In/Out of phase)	T1	3D	4.2/2.4	380 x 368	9	3	Column	675
	Volume interpolated GRE	T1	3D	4.4/2.1	340 x 340	9	2	Row	400
	Volume interpolated GRE (Dixon)	T1	3D	4.4/1.2	380 x 380	9	3	Column	975
	Single shot	T2	2D	900/87	340 x 340	120	3	Row	505

TSE								
TSE	T2	2D	4780/81	340 x 340	80	3	Column	230

Abbreviations: GRE = Gradient Echo sequence; SE = Spin echo sequence; TSE = Turbo Spin Echo; TR = Repetition Time; TE = Echo Time; BW = Bandwidth

[a] Maximum gradient strength 66 mT/m, slew rate 160 T/m/s

[b] Maximum gradient strength 30 mT/m, slew rate 125 T/m/s

[c] Maximum gradient strength 45 mT/m , slew rate 200 T/m/s

[d] Maximum gradient strength 45 mT/m, slew rate 200 T/m/s

II.D. Distortion analysis

MATLAB code was developed in-house and implemented to determine the position of each phantom grid point in the x and y planes. Each image was converted into a binary image by manually altering the threshold value so that all grid points could be differentiated from each other and any noise present in the image. The code was designed to calculate the central positions of each of these points. The distortion for each grid point was expressed as a function of its radial distance from scanner isocentre by comparing the positioning of the centre of the phantom relative to isocentre. Comparisons of distortion magnitude and patterns from isocentre were then undertaken for all sequences and scanners. The distortion magnitude was assessed relative to 2 mm.

II.E. Bandwidth Investigation

The effects of changing bandwidth on the distortion and signal to noise ratio (SNR) follow the relationship displayed in equation 1.

$$SNR \propto \frac{1}{\sqrt{receiver\ bandwidth}} \propto Distortion \qquad (1)$$

Scans were conducted on the Siemens 1.5 T MAGNETOM® Symphony Syngo scanner, for both visual and quantitative analysis of this relationship. The acquisition sequence utilised was a standard T1 weighted spin echo with TE = 30 ms, TR = 500 ms, FOV = 340 x 340 mm, slice thickness = 4 mm and echo train length = 1. The impact of varying both the bandwidth and the phase encoding direction was assessed. The receiver bandwidths investigated were 7.7, 25.6, 51.2, 76.8 kHz and 200 kHz with the readout gradient tested both in the anterior-posterior and right-left directions for each bandwidth value.

The impact on SNR with changing bandwidth was calculated from equation 2.

$$SNR = \frac{average\ signal}{std.deviation\ of\ background} \qquad (2)$$

The signal was calculated for each bandwidth by analysing twenty predetermined grid point regions of interest (ROI's) selected across the phantom area. The image noise was also sampled with ROI's of the same size across the background of each image.

II.F. Homogeneity assessment

The homogeneity of the central scanner region was assessed across a range of different areas across the central imaging plane of the scanner. Comparisons were made between the differences in distortion values for short to long bandwidth values. This was tested on the Siemens 1.5 T scanner. This was based on the work of Chen et al., utilising the following for expressing H_B [21]:

$$H_B(ppm) = \frac{BW_1 \cdot BW_2 \cdot (x_1' - x_2')}{(\gamma/2\pi) \cdot B_0 \cdot FOV \cdot (BW_2 - BW_1)} \quad (3)$$

where $\gamma/2\pi$ = 42.576 MHz/T for protons, BW_1 and BW_2 are the bandwidths of the data sets being compared, x_1 and x_2 are the coordinates in the frequency encoding direction of corresponding grid points for each bandwidth, B_0 is the main magnetic field strength and FOV is the field of view. The values were determined for a number of circular areas of varying diameters within the imaging plane.

II.G. Anatomical locations

Seven anatomical sites of interest for radiotherapy treatment planning were investigated to determine their common location with respect to the distance from the centre of both 60 cm and 70 cm bore MRI scanners. Contoured radiotherapy CT data sets of the breast, lung, oral cavity, larynx, brain stem, prostate and cervix were obtained for ten patients. In-house MATLAB code was utilised to determine the coordinates of the centre and extent of each contoured volume in the x and y planes.

The maximum radial distance that each anatomical contour extended from the scanner isocentre was recorded. It should be noted that the head and neck structures were based on CT scans obtained with the clinical radiotherapy set up practiced in the department where the region is elevated off the couch top.

III. RESULTS

III.A. Sequence and scanner distortion comparison

Figures 2 and 3 compare the distortion distribution for the different sequences and scanners investigated. The average distortion of the markers across the phantom area was less than 2 mm for the sequences tested. An increase in distortions above 2 mm generally occurred as the radial distance from isocentre extended beyond 100 mm. Due to the variations in bore size, the phantom was located closer to the edge of the bore, extending further from the isocentre in the 60 cm bore scanners in comparison to the 70 cm. This created a discrepancy between the maximum radial distances that could be assessed between the scanners.

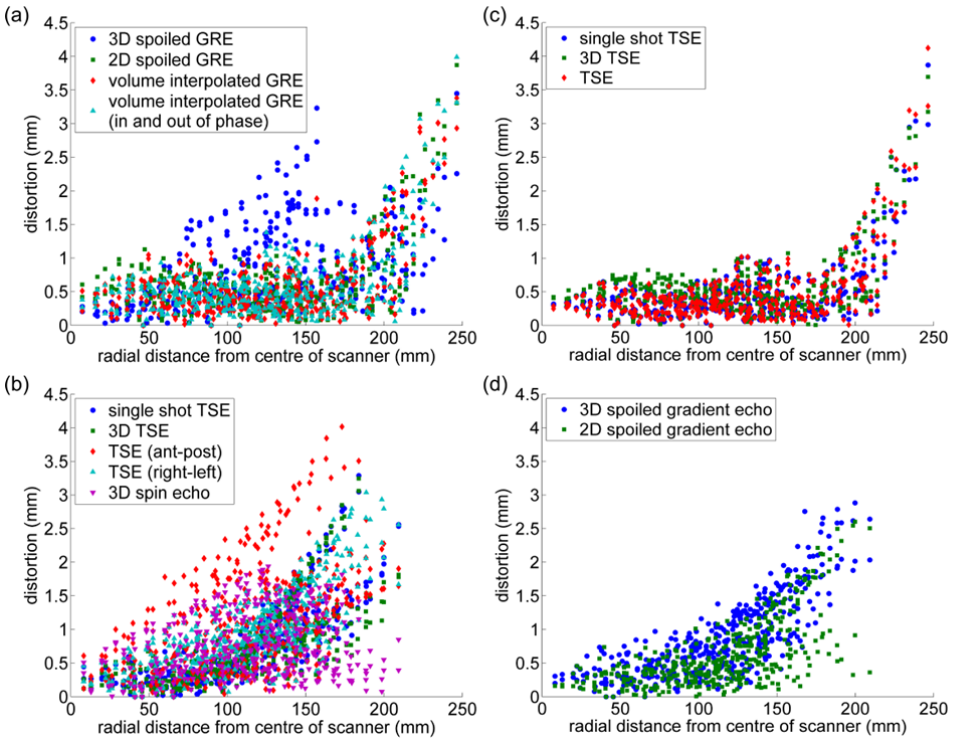

Fig. 2 Distortion distribution across the phantom area on the 1.5 T scanners for a. Philips Intera gradient echo sequences; b. Siemens Syngo gradient echo sequences; c. Philips Intera spin echo sequences; and d. Siemens Syngo spin echo sequences

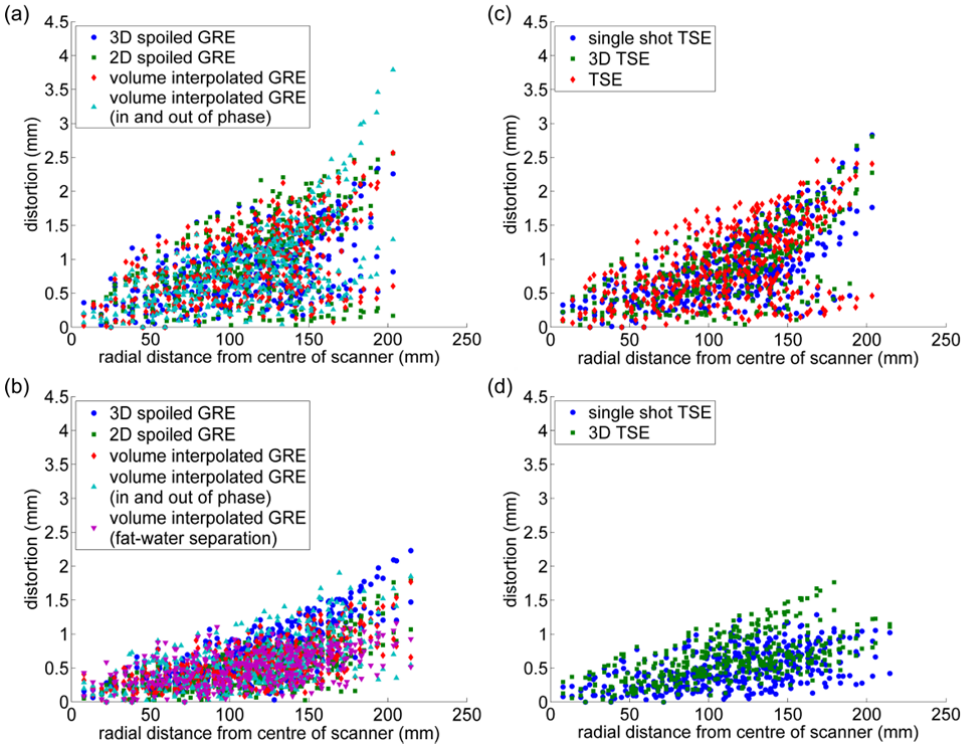

Fig. 3 Distortion distribution across the phantom area on the 3 T scanners for a. the Siemens Verio gradient echo sequences (2D correction applied); b. Siemens Skyra gradient echo sequences (2D correction applied); c.

Siemens Verio spin echo sequences (2D correction applied); and d. Siemens Skyra spin echo sequences (2D correction applied)

III.B. Bandwidth analysis

Table 2 shows the variation in average and maximum distortion values for the various receiver bandwidth values and the corresponding readout direction. The SNR for bandwidths between 7.68 kHz to 76.8 kHz ranged from 20 to 6.5, respectively. Bandwidths greater than this were not assessed due to the poor signal to noise observed in the images. For a bandwidth of 200 kHz, the SNR was reduced to 3.7, preventing the calculation of grid point locations. The homogeneity of the scanner was less than 0.4 ppm across areas with diameters ranging from 12 cm to 20 cm. On the 1.5 T scanner, a variation of 0.4 ppm in the magnetic field strength accounts for a distortion of 0.85 pixels for a bandwidth of 7.68 kHz. In these images, that equates to 1.13 mm distortion. For a receiver bandwidth of 76.8 kHz, this value is reduced to a distortion of 0.08 pixels (0.11 mm). The ratio between the measured distortion and that calculated to result from the B_0 field inhomogeneity indicates that increasing the receiver bandwidth results in the gradient nonlinearities being the predominate cause of distortions. When the bandwidth is reduced, the effect of these nonlinearities is reduced to around that resulting from the inhomogeneities in B_0.

Table 2 Comparison of the effects on the distortion values measured across the phantom for variations in the receiver bandwidth and phase encoding direction

Bandwidth (kHz)	Phase encode direction	Average distortion (mm ± SD)	Maximum distortion (mm)	SNR
7.7	Ant - Post	2.16 ± 1.66	6.33 ± 0.66	20.01
7.7	Right - Left	2.21 ± 1.48	5.27 ± 0.66	
25.6	Ant - Post	0.80 ± 0.57	3.00 ± 0.66	11.29
25.6	Right - Left	0.68 ± 0.45	2.16 ± 0.66	
51.2	Ant - Post	0.77 ± 0.44	2.23 ± 0.66	7.69
51.2	Right - Left	0.59 ± 0.37	1.96 ± 0.66	
76.8	Ant - Post	0.60 ± 0.36	1.93 ± 0.66	6.54
76.8	Right - Left	0.60 ± 0.37	1.74 ± 0.66	

III.C. Vendor 2D corrected vs. non-corrected images

Figure 4 shows the variations observed in changes in distortion magnitude and distribution across the phantom area with the application of the 2D correction algorithm for both a spin echo and gradient spin echo sequence. With the correction algorithm, both the average and maximum distortion values were minimised in some areas but were not completely removed. In some regions of the phantom, the distortion actually became worse with the 2D correction algorithm applied as opposed to without. Whilst the average distortions across the phantom area were all reduced to below 1.5 mm with the correction algorithm, the maximum distortions still remained greater than 2 mm, increasing with increasing distance from the isocentre. The performance of the correction algorithm with respect to radial distance from the scanner isocentre is highlighted in table 3. Figure 5

shows a distortion vector map comparing the difference in distortion between the grid point locations as seen with and without the correction algorithm applied. This shows the algorithm is not required to work as hard at smaller radial distances where distortions were generally found to be below 2 mm.

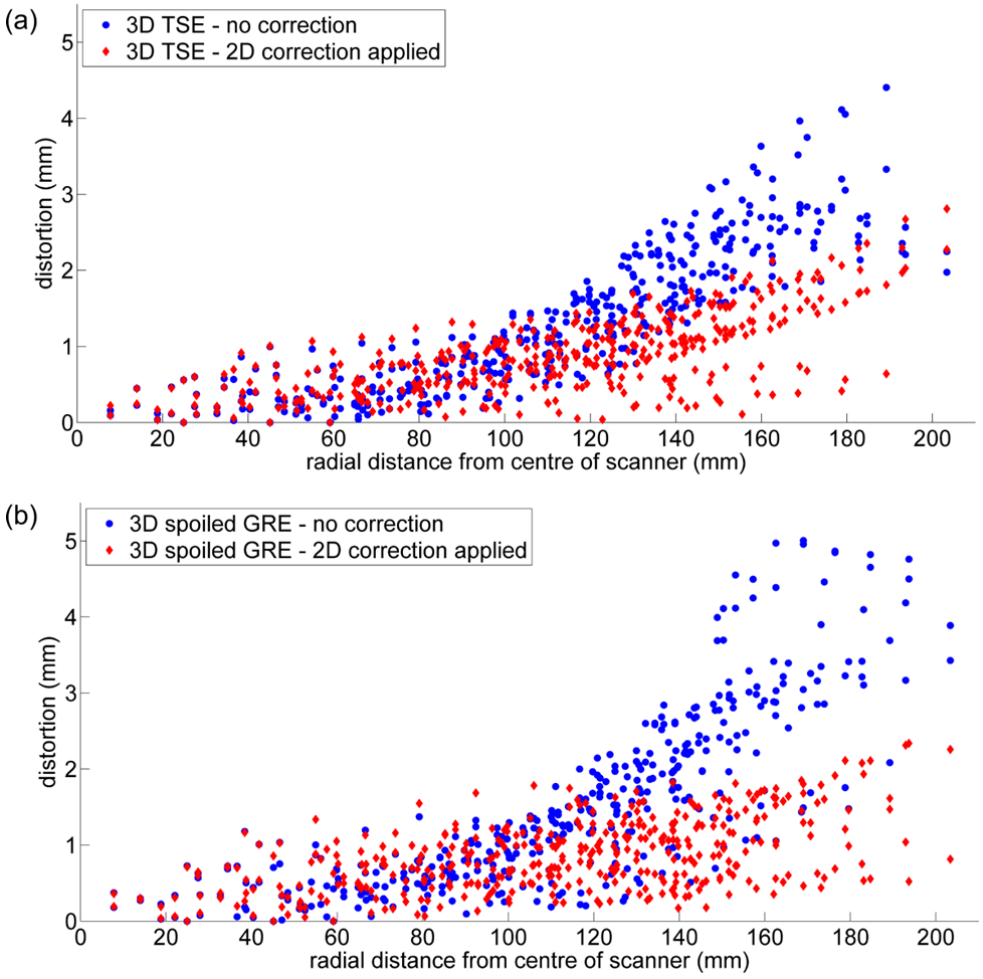

Fig. 4 Comparison of the distortion distribution across the phantom area with and without the application of the 2D correction for a. 3D turbo spin echo sequence and; b. 3D spoiled gradient echo sequence

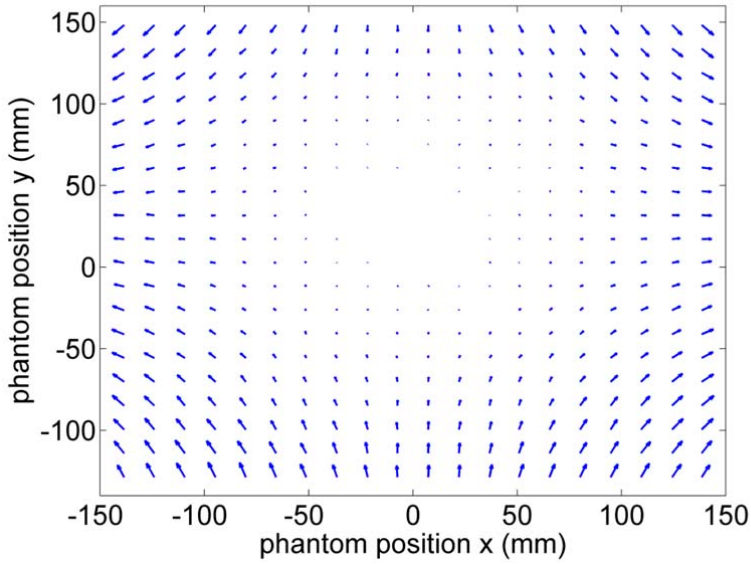

Fig. 5 Difference between 2D distortion maps of a 2D spoiled gradient echo sequence on a Siemens Verio 3 T scanner with and without the 2D correction algorithm applied

Table 3 Comparison of the variation in mean and average distortions observed for radial distances above and below 100 mm from the scanner isocentre

Sequence	Mean distortion (mm)		Maximum distortion (mm)	
	Below 100 mm	Above 100 mm	Below 100 mm	Above 100 mm
3D TSE				
- Corrected	0.53	1.09	1.32	2.81
- Non Corrected	0.47	1.86	1.19	4.41
3D spoiled GRE				
- Corrected	0.61	1.01	1.68	2.34
- Non Corrected	0.56	2.03	1.37	5.00

III.D. Anatomical locations

Figure 6 displays the distortion obtained on both Philips and Siemens T2 weighted turbo spin echo sequences with reference to the determined mean locations of the breast, lung, cervix, prostate and head and neck structures relative to the isocentre within a 2D axial imaging plane. The length of each represents the regions where each anatomical feature lies with respect to the centre of the scanner. The breast was the only anatomical structure investigated where the contour did not pass through the scanner isocentre.

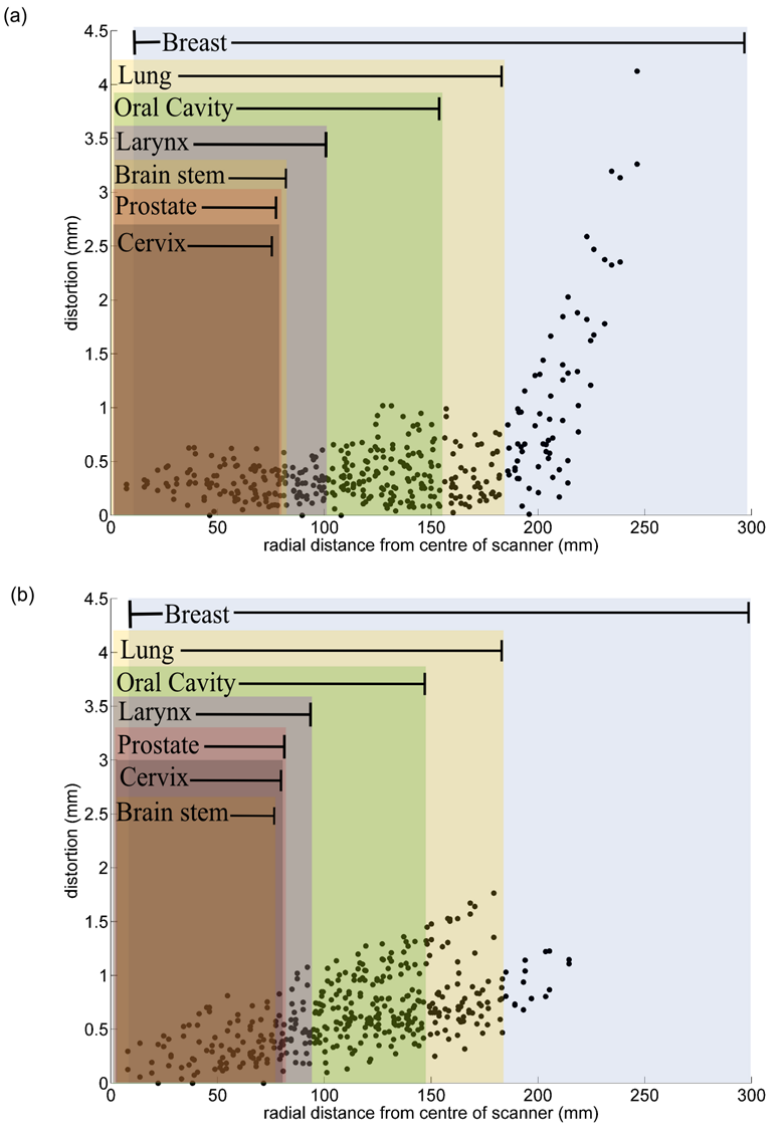

Fig. 6 The distortion observed from the radial distance from the centre of a. the Philips 1.5 T 60 cm bore scanner with the TSE sequence and; b. the Siemens 3T 70 cm bore Verio scanner. The blocks indicate the corresponding position of anatomical sites within the scanner. Note the scale has been extended out to illustrate where the breast is situated, although distortion measurements were not made beyond a radial distance of 250 mm. NOTE: The height of each box is for display purposes only and does not reflect any information regarding the distortion values.

IV. DISCUSSION

Each MRI acquisition sequence was demonstrated to be subject to individual distortion patterns as shown in Figs. 2 and 3. Parameter selection impacts the amount of distortion in an image. Equivalent sequences conducted on different scanners have varying distortion patterns. This is due to the system hardware design specification variations between vendors.

MRI scanners are optimised to exhibit least distortion towards the centre of the scanner, with the homogeneity and gradient linearity deteriorating with increasing radial distance from the centre. In this study, the phantom extended closer to the edge of the bore for the 60 cm bore scanners than those with 70 cm bores, due to the size limitations and fixed couch height. This was one of the reasons for the variations seen in the maximum distortions observed between the 60 and 70 cm bore scanners, all of which are capable of imaging a 50 x 50 cm FOV. This set up was the same as that used for current radiotherapy treatment planning MRI set up.

Receiver bandwidth is one parameter that effects MR image distortion as shown in table 2. A tenfold increase in receiver bandwidth saw a reduction in average distortion of more than 1 mm, while maximum distortions were reduced by more than 3 mm. A tenfold increase in this bandwidth resulted in a reduction in SNR of 13.5. To overcome this reduction in SNR, the number of excitations during the image acquisition may need to be increased. This may be a solution for phantom studies however applying this to the acquisition of patient images may not be practical with a resulting increase in total scan time and associated increase in motion artifacts. While smaller receiver bandwidth values result in better SNR, higher bandwidths result in less geometric distortion.

The homogeneity values obtained were based on the calculation method from Chen et al. [21]. The H_B value calculated of < 0.4 ppm across the scanner is consistent with the scanner specifications, which state the homogeneity across a 40 cm DSV is 0.4 ppm with a field stability of < 0.1 ppm/hour. One of the assumptions made in the calculations however, is that the gradients are linear, which is not the case particularly as the DSV increases.

For treatment planning purposes, vendor correction algorithms for gradient nonlinearities should be utilised on scanners with such capabilities in order to take advantage of their inbuilt distortion reduction software. Figures 4 and 5 show the difference in distortion values for images acquired with and without the correction algorithms applied, across the phantom area. It can be observed that in some regions both the magnitude and direction of the distortion is altered with the application of the correction algorithm, though the distortions were not completely removed.

One of the limitations of this study was the phantom utilised due to its shape and size. Firstly, because of the square shape within the cylindrical bore, there was a large region of the scanner, where distortion information could not be assessed. Since some patient anatomy (e.g. breast) may lie beyond this point, the phantom was insufficient for complete distortion analysis for RTP purposes. Secondly, the 2D grid structure only allowed for distortion assessment in one imaging plane. On scanners with distortion correction capabilities, the 2D correction algorithm was applied. Due to the phantoms structure, application of a 3D correction algorithm provided no additional benefit in terms of distortion reduction within the imaging region. The phantom was not rotated within the scanner to obtain 2D distortion data within other imaging planes.

A phantom for testing geometric distortion and field homogeneity would ideally consist of a number of points isolated in known positions in all three image planes, extending out over the entire FOV. This would be more representative of the regions within which the overall patient outline and anatomical regions of interest for

RTP would be located. Assessment of patient specific distortions (which have not been investigated in this study) would require the testing of additional anthropomorphic phantoms or patient data sets to determine the consequential variations in the local magnetic field values.

The variation in distortion distribution for clinical imaging sequences as observed in Figs. 2 and 3, demonstrates the importance of knowing the scanner specifications and the protocols used in the imaging process for use in RTP. Considerations should be made as to the possible affect that this may have on contouring uncertainties and dosimetric variations. In a clinical setting, these acquisition parameters are readily changeable in order to obtain an image of required quality for the purposes of planning, however the trade-offs between SNR and distortion values need to be considered. It was assumed for each acquisition sequence, with the same setup that the distortion values were reproducible [23].

The distortion maps in Figs. 2 and 3 can be compared to the position within which various clinical sites lie with respect to the centre of the scanner (Fig. 6). Since distortions are largest in the peripheral regions of the scanner, the impact on RTP may be of greater importance for anatomical structures situated in this region. Based on anatomical positioning within the scanner, treatment planning for the lung and breast clinical sites using MR images would have the largest distortion values to be considered. The distortions present in head and neck images would need to be considered, since the oral cavity may be a target volume or organ at risk. Patient contours are fundamental in the treatment planning process for the dose calculations. As such the extent of the patient within the scanner needs consideration. For breast patients, the breast contours also mark the extent of the patient contour. For the prostate and cervix, the overall patient contour can extend beyond a radial distance of 200 mm. For head and neck sites, the region of interest for the patient contour is reduced to below a radial distance of 150 mm from isocentre.

While MRI can be co-registered to the planning CT and incorporated in the RTP workflow [24], there is widespread interest in performing MR-only planning. MRI-only planning has the potential to decrease the ionising radiation exposure to the patient and, if both modalities are being utilised, the patient scan time. Additionally, CT-MRI registration may also introduce errors into the treatment planning process. Assessment of the geometric distortion is one important aspect to investigate when considering the use of MRI alone for planning, to ensure that the planning process and eventual treatment are accurate.

A number of points can be drawn for practical application for radiotherapy treatment planning from this study. The distortion and image quality of MRIs depends on parameter selection in the acquisition of the images and the specific scanner considered. As such the systematic related distortions should be measured for each sequence. Distortion variations across the imaging FOV results in clinical RTP sites experiencing varying degrees of distortion. The impact of this should be assessed on a site by site basis, being mindful of the acquisition sequences and associated parameters utilised.

V. CONCLUSION

This work provides a baseline assessment of variations in magnitude and distribution of systematic distortions present in MR images, comparing sequences and MRI scanners. These variations are due to the parameters utilised in the acquisition process. Selection of imaging protocol parameters is fundamental in any distortion investigation, particularly when considering the use of RTP planning with MRI alone. Depending on the clinical site of interest, the magnitude of distortions varies such that sites specific assessment of the possible clinical impact and potential correction of the distortions can be appropriately assessed.

ACKNOWLEDGEMENTS

The author would like to thank Michael Jameson from Liverpool Cancer Therapy Centre for useful discussions and access to some in-house code utilised in part of this project, as well as Peter Greer from the Calvary Mater Hospital Newcastle for access to the phantom. Special thanks to Matthew Hundy (Wollongong hospital), Joseph Turner (Campbelltown hospital) and Michael Serratore (Liverpool hospital) for their time in allowing access to the clinical MRI scanners to conduct this study.

1. Khoo VS, Dearnaley DP, Finnigan DJ, Padhani A, Tanner SF, Leach MO (1997) Magnetic resonance imaging (MRI): considerations and applications in radiotherapy treatment planning. Radiotherapy and Oncology 42 (1):1-15. doi:Doi: 10.1016/s0167-8140(96)01866-x

2. Chen L, Price JRA, Wang L, Li J, Qin L, McNeeley S, Ma CMC, Freedman GM, Pollack A (2004) MRI-based treatment planning for radiotherapy: Dosimetric verification for prostate IMRT. International Journal of Radiation Oncology*Biology*Physics 60 (2):636-647. doi:DOI: 10.1016/j.ijrobp.2004.05.068

3. Prabhakar R, Julka PK, Ganesh T, Munshi A, Joshi RC, Rath GK (2007) Feasibility of using MRI alone for 3D Radiation Treatment Planning in Brain Tumors. Japanese Journal of Clinical Oncology 37 (6):405-411

4. Baldwin LN, Wachowicz K, Thomas SD, Rivest R, Fallone BG (2007) Characterization, prediction, and correction of geometric distortion in 3 T MR images. Medical Physics 34 (2):388-399. doi:10.1118/1.2402331

5. Jezzard P (2009) The physical basis of spatial distortions in magnetic resonance images. In: Bankman IN (ed) Handbook of Medical Image Processing and Analysis. Second edn. Elsevier, pp 499-514

6. Chang H, Fitzpatrick JM (1992) A technique for accurate magnetic resonance imaging in the presence of field inhomogeneities. Medical Imaging, IEEE Transactions on 11 (3):319-329

7. Doran SJ, Charles-Edwards L, Reinsberg SA, Leach MO (2005) A complete distortion correction for MR images: I. Gradient warp correction. Physics in Medicine and Biology 50 (7):1343

8. Crijns SPMaR, B.W. and Lagendijk, J.J.W. (2011) Real-time correction of magnetic field inhomogeneity-induced image distortions for MRI-guided conventional and proton radiotherapy. Physics in Medicine and Biology 56 (1):289-297

9. Wang D, Doddrell DM, Cowin G (2004) A novel phantom and method for comprehensive 3-dimensional measurement and correction of geometric distortion in magnetic resonance imaging. Magnetic Resonance Imaging 22 (4):529-542. doi:DOI: 10.1016/j.mri.2004.01.008

10. Mizowaki T, Nagata Y, Okajima K, Kokubo M, Negoro Y, Araki N, Hiraoka M (2000) Reproducibility of geometric distortion in magnetic resonance imaging based on phantom studies. Radiotherapy and Oncology 57 (2):237-242. doi:Doi: 10.1016/s0167-8140(00)00234-6

11. Karger CP, Höss A, Bendl R, Canda V, Schad L (2006) Accuracy of device-specific 2D and 3D image distortion correction algorithms for magnetic resonance imaging of the head provided by a manufacturer. Physics in Medicine and Biology 51 (12):N253
12. Antolak JA, Rosen, II (1999) Planning target volumes for radiotherapy: how much margin is needed? International journal of radiation oncology, biology, physics 44 (5):1165-1170
13. Janke A, Zhao H, Cowin GJ, Galloway GJ, Doddrell DM (2004) Use of spherical harmonic deconvolution methods to compensate for nonlinear gradient effects on MRI images. Magnetic Resonance in Medicine 52 (1):115-122. doi:10.1002/mrm.20122
14. Baldwin LN, Wachowicz K, Fallone BG (2009) A two-step scheme for distortion rectification of magnetic resonance images. Medical Physics 36 (9):3917-3926
15. Bakker CJG, Moerland MA, Bhawandien R, Beersma R (1992) Analysis of machine-dependent and object-induced geometric distortion in 2DFT MR imaging. Magnetic Resonance Imaging 10 (4):597-608. doi:Doi: 10.1016/0730-725x(92)90011-n
16. Petersch B, Bogner J, Fransson A, Lorang T, Pötter R (2004) Effects of geometric distortion in 0.2 T MRI on radiotherapy treatment planning of prostate cancer. Radiotherapy and Oncology 71 (1):55-64. doi:DOI: 10.1016/j.radonc.2003.12.012
17. Stanescu T, Jans HS, Wachowicz K, Fallone BG (2010) Investigation of a 3D system distortion correction method for MR images, vol 11. 2010, vol 1.
18. Teodor Stanescu JH-S, Pavel Stavrev, B. Gino Fallone (2006) 3T MR-based treatment planning for radiotherapy of brain lesions. Radiology and Oncology 40 (2):125-132
19. Crijns SPM, Bakker CJG, Seevinck PR, Leeuw Hd, Lagendijk JJW, Raaymakers BW (2012) Towards inherently distortion-free MR images for image-guided radiotherapy on an MRI accelerator. Physics in Medicine and Biology 57 (5):1349
20. Zhang B, MacFadden D, Damyanovich AZ, Rieker M, Stainsby J, Bernstein M, Jaffray DA, Mikulis D, Menard C (2010) Development of a geometrically accurate imaging protocol at 3 Tesla MRI for stereotactic radiosurgery treatment planning. Physics in Medicine and Biology 55 (1):6601-6615. doi:doi:10.1088/0031-9155/55/22/002
21. Chen H-H, Boykin RD, Clarke GD, Roby J-HTGJW, III (2006) Routine testing of magnetic field homogeneity on clinical MRI systems. Medical Physics 33 (11):4299-4306
22. AAPM (1990) Quality assurance methods and phantoms for magnetic resonance imaging: Report of AAPM nuclear magnetic resonance Task Group No. 1. Medical Physics 17 (2):287-295. doi:10.1118/1.596566
23. Moerland MA (1996) Magnetic Resonance Imaging in Radiotherapy Treatment Planning. University Utrecht,
24. Devic S (2012) MRI simulation for radiotherapy treatment planning. Med Phys 39 (11):6701-6711. doi:10.1118/1.4758068